Blume-Capel model for $(Fe_{0.65}Ni_{0.35})_{1-x}Mn_x$ and $Fe_pAl_qMn_x$ alloys

D. Peña Lara,[1,*] G. A. Pérez Alcázar,[1] Ligia E. Zamora,[1] and J. A. Plascak[2,3]
[1]*Departamento de Física, Universidad del Valle, A.A. 25 360, Santiago de Cali, Colombia*
[2]*Departamento de Física, Universidade Federal de Minas Gerais, CP 702, Belo Horizonte 30 161-970, MG, Brazil*
[3]*Center for Simulational Physics, University of Georgia, Athens, Georgia 30602, USA*
(Received 8 May 2009; revised manuscript received 30 June 2009; published 24 July 2009)

A random-bond Blume-Capel model is proposed in order to study the ternary FeNiMn and FeAlMn alloys. The extended mean-field renormalization group approach and a variational procedure based on Bogoliubov inequality for the free energy are employed in the pair approximation. The phase diagrams are obtained for a symmetric distribution as well as for asymmetric distributions compatible to these alloys. The obtained phase diagram for the FeNiMn system is in a much better accord with the experimental data than the previous traditional mean-field renormalization group applied to the Ising model, mainly concerning the spin-glass and antiferromagnetic phases. Better results are also achieved for the order parameter of the FeAlMn alloys.

DOI: 10.1103/PhysRevB.80.014427 PACS number(s): 75.30.Kz, 75.50.Bb, 75.10.Dg

I. INTRODUCTION

Mechanical, corrosion/oxidation resistance, structural, and magnetic properties of ternary alloys have been hardly investigated in the past. The mechanical and corrosion/oxidation properties are useful, for instance, in applications to obtain stainless steel.[1–3] On the other hand, the magnetic and structural properties, which are the subject of this work, have been extensively studied by Mössbauer spectroscopy, x-ray diffraction, and magnetic susceptibility for FeNiMn alloys[4–7] and FeAlMn alloys.[8–11] The FeNiMn alloys are systems in which an atomic spin can interact with its neighbor atoms given an effective exchange interaction.[4,5] This interaction can be positive, negative, or nearly zero; therefore, paramagnetic (P), ferromagnetic (F), antiferromagnetic (AF), pure-spin glass (SG), and reentrant-spin glass (RSG) phases can be obtained and have already been experimentally reported in the literature.[5,6] Concerning the FeAlMn alloys it has been shown that these systems exhibit an antiferromagnetic behavior with a nearly constant mean hyperfine field of $\bar{H}=26$ kOe, in the composition range given by $0.5<p<0.65$ and $0<q<0.075$, where p and q are, respectively, the iron and aluminum concentrations of a general $Fe_pAl_qMn_x$ alloy, where $x=1-p-q$.[9]

In order to explain some of the magnetic properties of these alloys it has been used well-known Ising-like models in both diluted and competitive versions.[7,8,12–14] An analytical treatment based on Bogoliubov procedure for the free energy in the pair approximation,[15] as well as mean-field renormalization group approaches,[16,17] have been employed and quite good agreement with the experimental data have been achieved.

So far, the proposed theoretical fittings have been based on a spin $S=1/2$ Ising model,[18,19] with the presence of an isotropic bilinear exchange interaction J_{ij} by considering an adequate probability distribution $P(J_{ij})$, which reasonably explains the continuous transition exhibited by these alloys in the disordered phase.[7,8,12] Although the bond diluted problem given by a distribution function $P(J_{ij})$ is simpler to be done than the actual site dilution considered, for instance, in Ref. 13, the theoretical results are qualitative the same. The comparison between the experimental data and the theoretical fittings have been, at least, reasonable, but there are still slight discrepancies in the behavior of the reduced mean hyperfine field as a function of Al, Mn, or Fe concentration for FeAlMn alloys, as well as some severe disagreements regarding the fittings of the spin-glass transition for the FeNiMn alloys. These disagreements could be associated to the magnetic anisotropy which is present in many magnetic materials and that is not taken into account in the Ising model. This is, in fact, the point we would like to address in the present study.

The thermodynamic properties of a magnetic system are subjected to electrostatic interactions due to the neighboring charges. It has long been known that these interactions, at least in first approximation, could be simulated by introducing a crystal field (CF) or zero-field splitting (ZFS) Δ.[20,21] The symmetry and strength of Δ affect the electronic levels of the system.[22] CF reduces the degeneracy (since there is no preferred orientation of the angular momentum and therefore no preferred orientation of the magnetic moment due to spin) of the electronic levels for two correlated electron spins in zero-field systems (ignoring the electron exchange interaction and only considering the magnetic interactions, for this reason the ZFS name) with $S\geq 1$ and causes magnetic anisotropy.[23–25]

In order to try to explain the discrepancies exhibited by the reduced mean hyperfine field as a function of Al, Mn, or Fe concentration for FeAlMn alloys and the spin-glass transition curve of FeNiMn system, and keeping in mind the CF or ZFS, as well as the electron exchange interaction, we intend to use a spin $S=1$ model in the new theoretical fittings. This system, which is an extension of the Ising model, has been introduced by Blume and Capel (BC)[26,27] in the context of tricritical phenomena. As we will shortly see this new model for such alloys gives remarkable account for the discrepancies previously obtained from the Ising spin system.

Thus, we consider a type of competing random-bond Blume-Capel model which is presented in Sec. II. In order to treat the continuous transitions of these systems we employ the extended mean-field renormalization group approach that is outlined in Sec. III. The results for the phase diagram by considering the symmetric probability distribution is pre-

 ©2009 The American Physical Society

sented in Sec. IV, while the application to the physical realization of FeNiMn alloys is discussed in Sec. V. In Sec. VI we report some fittings of the model applied to the FeAlMn disordered alloys. Some final comments and remarks are summarized in Sec. VII. Appendices A and B are devoted to convey some of the final theoretical expressions for the corresponding physical realizations.

II. RANDOM SPIN-*S* BLUME-CAPEL MODEL

In a magnetic system, we can have several kinds of interactions: spin-spin coupling, spin-orbit coupling, orbit-lattice coupling, etc. The spin-spin coupling is strong and keeps neighboring spins parallel or antiparallel. The spin-orbit coupling is related to the crystal anisotropy, i.e., the magnetic properties depend on the direction in which they are measured.[25] The orbit-lattice coupling is also strong and keeps the orientations of the orbits fixed strongly to the lattice. Of these couplings we are interested here in the first two, because the first coupling is related with ferromagnetism ($J_{ij}>0$) or antiferromagnetism ($J_{ij}<0$) and the second with the ZFS or CF.

The idea to remove the degeneracy for systems with spin $S\geq 1$ in the absence of an applied field arises from spin-orbit coupling of the ground state with empty excited states (for $S=1$, the ground-state $m_S=0, \pm 1$ is splitting into a singlet, $m_S=0$, and a doublet, $m_S=\pm 1$). The theory that tries to explain this phenomenology was developed by van Vleck[20,21] and Bethe,[22] and is known as crystal-field theory (CFT). This theory describes the effect of the electrical field of neighboring ions on the energies of the valence orbitals of an ion in a crystal and it can be used to predict chemical properties, kinetic properties, reaction mechanisms, magnetic and spectral properties, and thermodynamic data.

We take into account a reported theory for magnetic anisotropy[28] which assumes a Hamiltonian with exchange and crystal-field term given by

$$\underset{\text{Exchange}}{\sigma_i \cdot \underset{\sim}{\mathbf{J}}_{ij} \cdot \sigma_j} + \underset{\text{Crystal field}}{\sigma_i \cdot \underset{\smile}{\mathbf{D}} \cdot \sigma_i},$$

where the first term describes an interaction between spins σ_i and σ_j at two sites, and the second term involves the spin at only one site. The parameter $\mathbf{J}_{ij}$ and the third-rank tensor $\mathbf{D}$ describe the strength of the two-ion exchange interaction and single-ion spin-spin interaction, respectively.

Instead of working with tensors and keeping in mind the Bethe-Slater curve,[29] we will assume that the electronic ground state of these compounds can be viewed as a singlet ($m_s=0$), and a doublet level ($m_s=\pm 1$) lying at an energy Δ above the singlet. This picture is very similar to one which considers an Ising model consisting of triplet ions with zero-field splitting[26] or an Ising model in the presence of isotropic bilinear exchange and of crystal-field splitting of the proper magnitude and sign.[27]

Thus, we consider the Blume-Capel model defined by the following Hamiltonian:

$$H = -\sum_{\langle ij \rangle} J_{ij}\sigma_i\sigma_j + \Delta\sum_{i=1}^{N} \sigma_i^2, \tag{1}$$

where J_{ij} is the random nearest-neighbor (nn) coupling constant, Δ is the crystal anisotropy field and the first sum is over nearest-neighbor pairs on a lattice of N sites. The spin values σ_i are $-S,-S+1,\ldots,S-1,S$. For $J_{ij}=J$ and $S=1/2$ we have the spin-1/2 Ising model and when $S=1$, H corresponds to the model introduced by Blume[26] and Capel.[27] It was introduced by Blume to account for first- and second-order phase transitions observed in UO_2 assuming that U^{4+} ion consists of a nonmagnetic single ground state and a low-lying magnetic triplet, and that only bilinear isotropic exchange interactions are present. Capel applied it to the study of a system consisting of triplet ions with zero-field splitting and exchange interaction between nearest neighbors. This model is also used to describe tricritical phenomena observed in the metamagnetic system $Ni(NO_3)_2\cdot 2H_2O$,[30] ^{3}He-^{4}He mixtures,[31] the behavior of superconductor films,[32] Dysprosium Aluminum Garnet (DAG),[33] and a long list of other systems. Since no exact solution is known for $d\geq 2$ dimensions, this model has been extensively studied within several approximate schemes such as mean-field approximation,[26,27] Monte Carlo simulations,[34,35] renormalization group methods,[36,37] and conformal invariance,[38,39] among others.

The randomness in this model comes by assigning a probability distribution for the exchange interactions $P(J_{ij})$. As is usual in competing random-bond models, the simple symmetric distribution

$$P(J_{ij}) = p\,\delta(J_{ij}-J) + q\,\delta(J_{ij}+J), \tag{2}$$

where p is the probability of having ferromagnetic interactions J and $q=1-p$ is the probability of having antiferromagnetic interactions $-J$, is responsible for a symmetric spin-glass phase in the system. For asymmetric interactions, such as ferromagnetic interactions J and antiferromagnetic interactions $-J_1$, for example, the phase diagram has its symmetry broken regarding $p=1/2$.

For the particular case of the FeNiMn alloys discussed above, where p, q, and x are the Fe, Ni, and Mn concentrations, respectively, one can consider the following more general distribution:

$$P(J_{ij}) = p^2\delta(J_{ij}-J) + q^2\delta(J_{ij}-J_1) + x^2\delta(J_{ij}-J_2) + 2pq\,\delta(J_{ij}-J_3) + 2px\,\delta(J_{ij}-J_4) + 2qx\,\delta(J_{ij}-J_5), \tag{3}$$

where p^2 is the probability of having two nn Fe atoms with an exchange interaction $J\equiv J_{\mathrm{FeFe}}$, q^2 represents the probability between two Ni atoms with $J_1\equiv J_{\mathrm{NiNi}}$, x^2 is the bound probability between Mn atoms having $J_2\equiv J_{\mathrm{MnMn}}$, $2pq$ is the probability between Fe-Ni atoms with $J_3\equiv J_{\mathrm{FeNi}}$, and $2px$ and $2qx$ represent the probability between Fe-Ni and Ni-Mn atoms having an exchange $J_4\equiv J_{\mathrm{FeNi}}$ and $J_5\equiv J_{\mathrm{NiMn}}$, respectively. In this case one also has $p+q+x=1$.

For the FeAlMn systems, where p, q and x are the Fe, Al, and Mn concentrations, respectively, we have

$$P(J_{ij}) = p^2\delta(J_{ij}-J) + x^2\delta(J_{ij}-J_2) + 2px\delta(J_{ij}-J_4) + q(2-q)\delta(J_{ij}), \quad (4)$$

where p^2 is the probability of having two *nn* Fe atoms with and exchange interaction $J \equiv J_{\mathrm{FeFe}}$, x^2 represents the probability between two Mn atoms having an exchange $J_2 \equiv J_{\mathrm{MnMn}}$, $2px$ is the probability between Fe-Mn atoms with $J_4 \equiv J_{\mathrm{FeMn}}$ and the last term, $q(2-q)$, represents all the possible diluted bonds with nonmagnetic Al sites (Fe-Al, Mn-Al, and Al-Al), i.e., $J_1 \equiv J_{\mathrm{AlAl}}=0$, $J_3 \equiv J_{\mathrm{FeAl}}=0$ and $J_5 \equiv J_{\mathrm{MnAl}}=0$, which are given by $q^2+2qp+2qx=q(2-q)$.

In order to get the second-order behavior of this system we have applied the extended MFRG procedure outlined in Ref. 36. A brief summary is given in the next section.

III. EXTENDED MFRG METHOD

The Mean-Field Renormalization Group (MFRG) method[40] has been applied to study nonclassical critical properties of lattice models.[41] However, when this method is applied to the spin $-S$ Ising model with $S \geq 1$, the results are not equivalent to the Bethe ones and, besides, one gets a critical temperature $T_c \neq 0$ for the one-dimensional model.[42,43] The extended MFRG is able to provide, using the smallest cluster, the same results for the critical temperature as those obtained from Bethe and constant coupling approximation.[44]

The extended MFRG method, in treating a magnetic system, considers two clusters of interacting spins containing N and N' sites, with $N' < N$. The magnetizations per spin (order-parameter $m=\langle\sigma\rangle$) $m_N(K,D,q,b)$ and $m_{N'}(K',D',q',b')$ are computed for both clusters, where K is the reduced exchange interaction, D is a parameter of the Hamiltonian, and q and b are the symmetry-breaking fields. In the present model we have, for instance, $K=\beta J$ and $D=\beta\Delta$, where $\beta=1/k_BT$ with k_B the Boltzmann constant. Close to a second-order phase transition the magnetization of the system is very small and assuming that $b \ll 1$ and $b' \ll 1$ we can expand $m_N(K,D,q,b)$ and $m_{N'}(K',D',q',b')$ up to first-order in b and b', respectively, to obtain

$$m_{N'}(K',D',q',b') = f_{N'}(K',D',q')b', \quad (5)$$

$$m_N(K,D,q,b) = f_N(K,D,q)b. \quad (6)$$

Using appropriate scaling relation for the approximate magnetizations and symmetry-breaking fields, namely, $m_{N'}=\ell^{\phi}m_N$ and $b'=\ell^{\phi}b$, where $\ell=(N/N')^{1/d}$ is the scaling factor with d the dimension of the lattice and ϕ is the anomalous dimension of the order parameter, one gets

$$f_{N'}(K',D',q') = f_N(K,D,q). \quad (7)$$

Note that for models as the one given by Eq. (1), the breaking fields q and q' are related to noncritical variables. In the present case they correspond to the quadrupole quantity $Q=\langle\sigma^2\rangle$. Regarding this quantity as having zero anomalous dimension it means that one has[45]

$$Q_{N'}(K',D',q',b'=0) = Q_N(K,D,q,b=0) \quad (8)$$

and

$$q' = q. \quad (9)$$

Equations (7)–(9) give the second-order phase transition by restricting the parameter space to the physical plausible invariant subset $D'=D$. It should be stressed here that, for quenched random systems, the magnetizations m and quadrupoles Q should also be averaged with respect to the bond probability distribution.

To study the presence of possible spin-glass phases one resorts to the Edwards-Anderson order parameter. It is given by $g=\overline{\langle\sigma\rangle^2}$, where the brackets mean the thermal average, as before, and the overline means the configurational average over the random bonds. By following the same procedure as in Refs. 16, 46, and 47 one gets for the spin-glass order-parameter

$$g_{N'}(K',D',q',b') = h_{N'}(K',D',q')b'^2, \quad (10)$$

$$g_N(K,D,q,b) = h_N(K,D,q)b^2. \quad (11)$$

Assuming a similar scaling relation $g_{N'}=\ell^{\theta}g_N$ and $b'^2=\ell^{\theta}b^2$, where θ is the anomalous dimension of the spin-glass order parameter we have

$$h_{N'}(K',D',q') = h_N(K,D,q). \quad (12)$$

Accordingly, we can also compute the noncritical variable $R=\overline{\langle\sigma^2\rangle^2}$, from which we arrive at the relation

$$R_{N'}(K',D',q',b'^2=0) = R_N(K,D,q,b^2=0). \quad (13)$$

From Eqs. (12), (13), and (9) we get the spin-glass transition line.

In order to apply the above extended MFRG method to the model (1) we consider finite systems with one and two spins. Thus, the Hamiltonian for the one- and two-spin clusters can be written as

$$H_1 = -\sum_{i=1}^{z} J'_{1i}b'_i\sigma_1 + \Delta\sigma_1^2 - \sum_{i=1}^{z} q'_i\sigma_1^2, \quad (14)$$

$$H_2 = -J_{12}\sigma_1\sigma_2 - \sum_{i=1}^{z-1} J_{1i}b_{1i}\sigma_1 - \sum_{i=1}^{z-1} J_{2i}b_{2i}\sigma_2 + \Delta(\sigma_1^2+\sigma_2^2) - \sum_{i=1}^{z-1} q_i(\sigma_1^2+\sigma_2^2), \quad (15)$$

where z is the coordination number of the lattice. In the above equations b'_{1i} and $b'_{ni}(n=1,2)$ are the symmetry-breaking fields acting at the boundary of the respective cluster, which are related to the magnetization of the system $m=\langle\sigma\rangle$, and q'_i and q_i are additional parameters related to the quadrupole $Q=\langle\sigma^2\rangle$.

Therefore the magnetizations per spin for the one- and two-spin clusters are given by

$$m_1 = \overline{\langle\sigma_1\rangle_1}, \quad m_2 = \overline{\langle\sigma_1\rangle_2}, \quad (16)$$

where the thermal averages are given by

$$\langle\sigma_1\rangle_1 = \frac{\mathrm{Tr}[\sigma_1 e^{-\beta H_1}]}{\mathrm{Tr}[e^{-\beta H_1}]}, \quad \langle\sigma_1\rangle_2 = \frac{\mathrm{Tr}[\sigma_1 e^{-\beta H_2}]}{\mathrm{Tr}[e^{-\beta H_2}]}. \tag{17}$$

The corresponding bond distribution averages are computed from

$$\overline{\langle F(J_{ij})\rangle} = \int \prod_{ij} dJ_{ij} P(J_{ij}) \langle F(J_{ij})\rangle. \tag{18}$$

Similarly, for the quadrupole one gets

$$Q_1 = \overline{\langle\sigma_1^2\rangle_1}, \quad Q_2 = \overline{\langle\sigma_1^2\rangle_2}, \tag{19}$$

where

$$\langle\sigma_1^2\rangle_1 = \frac{\mathrm{Tr}[\sigma_1^2 e^{-\beta H_1}]}{\mathrm{Tr}[e^{-\beta H_1}]}, \quad \langle\sigma_1^2\rangle_2 = \frac{\mathrm{Tr}[\sigma_1^2 e^{-\beta H_2}]}{\mathrm{Tr}[e^{-\beta H_2}]}. \tag{20}$$

Regarding the spin-glass phase we have

$$g_1 = \overline{\langle\sigma_1\rangle_1^2}, \quad g_2 = \overline{\langle\sigma_1\rangle_2^2}, \tag{21}$$

and

$$R_1 = \overline{\langle\sigma_1^2\rangle_1^2}, \quad R_2 = \overline{\langle\sigma_1^2\rangle_2^2}. \tag{22}$$

Let us consider the spin-1 ($S=1$) spin-glass Blume-Capel model with the distribution (2). In this case, it is not so difficult to compute m_1, m_2, Q_1, and Q_2 from the Hamiltonians (14) and (15). After expanding for small fields b' and b, and using the MFRG relations (7)–(9) we obtain

$$\frac{2ze^{\delta_1}}{(z-1)Z_1} = \frac{e^{\delta_2} + 2pe^{2\delta_2+K} + 2(1-p)e^{2\delta_2-K}}{Z_2}, \tag{23}$$

$$\frac{2e^{\delta_1}}{Z_1} = \frac{2e^{\delta_2} + 4e^{2\delta_2}\cosh(K)}{Z_2}, \tag{24}$$

where $K=\beta J$, $\delta_1=-\beta\Delta+z\beta\gamma$, $\delta_2=-\beta\Delta+(z-1)\beta\gamma$, and the corresponding partition functions

$$Z_1 = 1 + 2e^{\delta_1}, \tag{25}$$

$$Z_2 = 1 + 4e^{\delta_2} + 4e^{2\delta_2}\cosh(K). \tag{26}$$

Equations (23) and (24) give the ferromagnetic phase boundary for high values of the concentrations p. For small p, we have more antiferromagnetic bonds and the system will be in an antiferromagnetic state. However, by considering two sublattices and treating the sublattice magnetization as order parameters we arrive at the same Eqs. (23) and (24) for the antiferromagnetic phase boundary with p replaced by q. In other words, the phase diagram of the Hamiltonian (1) is symmetric regarding $p=1/2$ for the random distribution (2).

The corresponding spin-glass phase boundary from Eqs. (12), (13), and (9) is given by

$$\frac{ze^{2\delta_1}}{(z-1)Z_1^2} = \frac{e^{2\delta_2} + 4e^{3\delta_2}\cosh(K) + 4e^{4\delta_2}\cosh(2K)}{Z_2^2}, \tag{27}$$

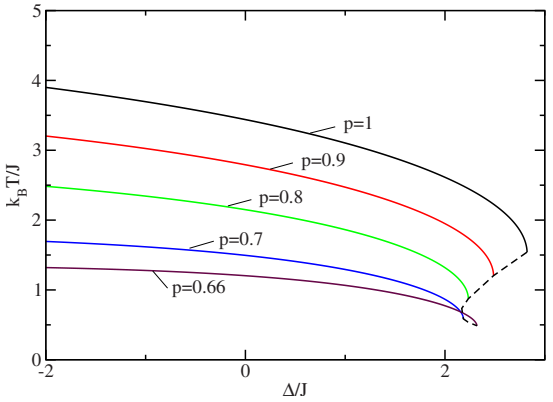

FIG. 1. (Color online) Reduced critical temperature as function of the reduced crystal field for different concentrations. The dashed line corresponds to the tricritical points.

$$\frac{4e^{2\delta_1}}{Z_1^2} = \frac{[2e^{\delta_2} + 4e^{2\delta_2}\cosh(K)]^2}{Z_2^2}. \tag{28}$$

It is interesting to notice that for the symmetric random-bond distribution (2) the spin-glass transition line is independent of the concentration p.

For the more general distribution (3) the corresponding equations for $S=1$ are given in the Appendix A. Similarly, the procedure can be extended for spin values $S>1$.

IV. SYMMETRIC DISTRIBUTION PHASE DIAGRAMS

Before treating the present alloys it is worthwhile to study the theoretical phase diagram of the spin-glass spin-1 Blume-Capel model on a three-dimensional simple-cubic lattice ($z=6$) according to the distribution (2) from the present extended MFRG approach. In this case, not only have we results in the literature for the Ising model to compare with, but also some recent study of the same model by a different renormalization group approach.[48] As the phase diagram in this case is symmetric regarding $p=1/2$, we will present results only for the ferromagnetic phase.

In Fig. 1 it is shown the reduced critical temperature (k_BT/J) of the second-order ferromagnetic transition line as a function of the reduced crystal-field ($d=\Delta/J$) for several concentrations p. The end of the second-order transition line is ascribed the tricritical point. For $p=1$ we recover the previous diagram of the spin-1 Blume-Capel model according to the extended MFRG.[45] There is a critical concentration $p_c = \frac{z}{2(z-1)}$ which suppresses the second-order transition line ($p_c=0.6$ for $z=6$). One can see that the tricritical crystal field decreases when the concentration decreases from $p=1$ to about $p=0.7$. Then, for smaller values of p, the crystal field increases. Differently, the tricritical temperature always decreases as the concentration of ferromagnetic bonds decreases. There is a line of tricritical points as the concentration changes with no fourth-order point.

Projections of the phase diagram on the reduced temperature versus concentration of ferromagnetic bonds plane for several values of the reduced crystal field are depicted in Fig. 2. For the sake of clarity only the ferromagnetic phase-

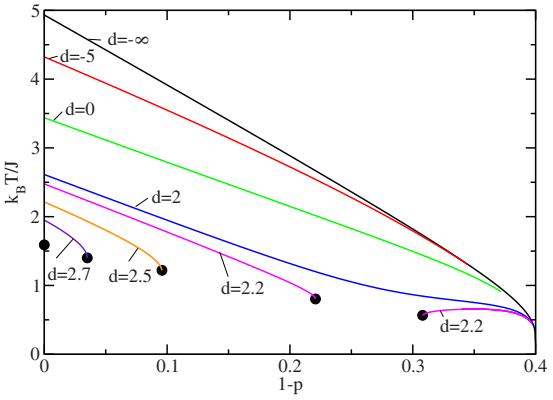

FIG. 2. (Color online) Reduced critical temperature as function of the concentration of ferromagnetic bonds for different crystal-field values. The dots correspond to the tricritical points. The tricritical point at $p=1$ occurs for $d=2.82$.

transition boundaries are shown. As expected, for $d\rightarrow-\infty$ one has the spin-1/2 Ising model with the same results reported in Refs. 16 and 47. As d increases the corresponding second-order transition line decreases and independently of the crystal field they go to zero at p_c for $d>2.48$. For $d<2.16$ the transition line is always second order. For $2.16<d<2.48$ one finds two tricritical points while for $2.48<d<2.82$ there is only one tricritical point. For $2.82<d<3$ we have only first-order transition lines which cannot be located from the extended MFRG because we do not have the free energy nor the magnetizations as a function of temperature.

Figure 3 depicts the reduced critical temperature as a function of concentration of ferromagnetic bonds for several values of the reduced crystal field including the transition from the spin-glass phase to the disordered phase. The spin-glass transition is independent of the concentration for the symmetric distribution (2). This is not the case when one considers asymmetric distributions. For $d>2.2$ there is no spin-glass phase. The inset in Fig. 3 shows the spin-glass transition temperature as a function of the crystal field.

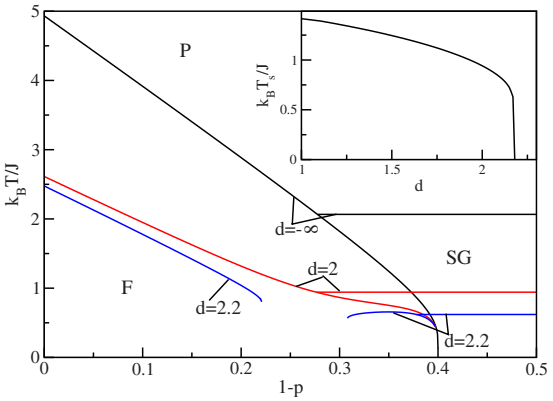

FIG. 3. (Color online) The same as Fig. 2 including the spin-glass transition lines which are concentration independent. F stands for ferromagnetic, P for paramagnetic, and SG for spin-glass phases. The inset shows the spin-glass transition temperature as a function of the reduced crystal field.

The above results are, in some range of the theoretical parameters, qualitatively the same as those recently reported for this same model.[48] However, we do not find, from our approach, any inverted tricritical points. Even so, we should mention that the experimental data do not present any inverted tricritical point and we believe that the present approximation is applicable for the range of theoretical parameters we need.

V. FE-NI-MN ALLOYS

Let us now turn our attention to the FeNiMn alloys. In this case, the $S=1$ Blume-Capel system can be suitable because $(Fe_{0.65}Ni_{0.35})_{1-x}Mn_x$ alloys present four states, and this model can be seen as an approximation to the random axis model (RAM) to describe amorphous magnetic materials.[49]

In order to reproduce the experimental magnetic phase diagram reported in Ref. 6 for this alloy system, we follow the $S=1$ Blume-Capel model according the extended MFRG method. To obtain the ferromagnetic phase boundary we used the expressions (A3)–(A6) of Appendix A, corresponding to the calculated magnetizations and to the quadrupoles for the one and two spins blocks, respectively. Similarly, in order to obtain the spin-glass boundary we used the expressions (A10)–(A13) of this Appendix, which correspond to the Edwards-Anderson spin-glass order parameters and to the quadrupoles for the one and two spins blocks, respectively. In our calculations the value for the parameters are $J\equiv J_{FeFe}=-2.05$ meV, $J_1\equiv J_{NiNi}=17.01$ meV, $J_2\equiv J_{MnMn}=-10.42$ meV, $J_3\equiv J_{FeNi}=5.92$ meV, $J_4\equiv J_{FeMn}=-4.63$ meV, $J_5\equiv J_{NiMn}=-5.32$ meV, and $\Delta=1$ meV. All these parameters are the same as those adjusted in Ref. 7, except the last one which was not included in their model. Two facts can be highlighted here which were also pointed out in Ref. 7: (1) the AF character of the bounds in which the Mn atom is present, associated to the large AF character of the Mn atom and (2) the AF character of the Fe-Fe bond as a consequence of the shorter *nn* distance in this fcc phase related to that of *nn* atoms in a bcc lattice (that of pure Fe).

The experimental and calculated phase boundaries using the theoretical parameters given above are plotted in Fig. 4, by dots and solid lines, respectively. For comparison we plotted in this figure, by dotted lines, the previous theoretical fitting reported in Ref. 7 obtained by using a simple diluted and random-bond Ising model within the MFRG method for blocks of one and two spins by considering the distribution given by Eq. (3). As can be noted in Fig. 4, the current theoretical boundaries show an excellent agreement with the experimental data and reproduce very well the four experimental magnetic regions reported experimentally. It can also be noted that in the previous work[7] only the boundaries between the RSG and F phases, and that between the F and P phases (for low Mn contents) present good agreement, while for the boundary between the SG and the P phases the disagreement is clearly apparent. From a closer inspection of Fig. 4 we have: (i) the F-P transition line from both approaches are almost the same, except close to the SG region where the present procedure gives a line almost perpendicular to the SG phase boundary while the Ising model predicts

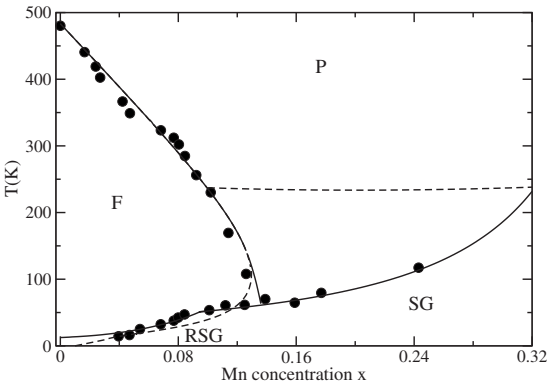

FIG. 4. Phase diagram for $(Fe_{0.65}Ni_{0.35})_{1-x}Mn_x$ (ternary system). The dots represent the experimental data (Ref. 6). The solid line is obtained by the present extended MFRG on the Blume-Capel model and the dotted line is the previous fitting from an Ising model (Ref. 7). Except from the crystal field, the parameters are the same for both models (see the text). The phases are ferromagnetic (f), paramagnetic (p), spin glass (SG), and reentrant spin glass (RSG).

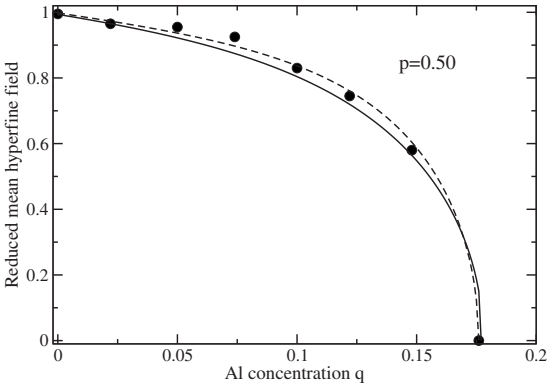

FIG. 5. Reduced mean hyperfine field as a function of Al concentration q at room temperature for Fe concentration $p=0.50$. Experimental data (full circles) are from Ref. 9 and the theoretical fitting from a simple Ising model (dashed line) are from Ref. 12. The solid line is obtained from the present Blume-Capel model with Eq. (29) and parameters given in the text.

a reentrancy in the P phase (the bold dotted line is an extrapolation from the full line); (ii) the F-RSG phase boundary is better fitted from the present BC model and as the Mn concentration goes to zero the critical temperature is higher than for the Ising model; (iii) the Ising model gives a SG-P transition line which almost constant at $T=250$ K, in complete disagreement with the experimental data; (iv) finally, not shown in that Figure for clarity reasons, the Ising model predicts a phase boundary between the SG and antiferromagnetic phase which has not been seem for these alloys (see Fig. 1 of Ref. 7). This can be associated to the crystal field and to the continuous stabilization of the SG phase due the increase in the AF bonds induced by the increase in Mn which compete with the two F ones due to Ni-Ni and Ni-Fe interactions).

VI. FE-AL-MN ALLOYS

In the preceding sections we have analyzed only the phase diagrams for the symmetric distribution and applied the asymmetric one to the ternary FeNiMn alloys phase diagram. The agreement with the experimental data was remarkable. Thus, it would be also interesting to see what happens to the present model when treating the order parameter of the Fe-AlMn alloys, where the Ising model gave already a good description of the order-parameter behavior as a function of the concentrations at room temperature. In this case, however, the system does not present the spin-glass phase and we can resort to a variational approach to seek for the disorder behavior of order parameter. This approach has been used before (see, for instance, Refs. 7 and 8) so in Appendix B we just outline the Bogoliubov procedure for the behavior of the magnetization as a function of temperature and concentrations.

Thus, we considered the distribution function given by Eq. (4). In addition, we also have to take into account that the exchange parameter J is a decreasing function of Al concentration q. This can be achieved by assuming

$$J(q) = J_1 - qJ_0, \tag{29}$$

where J_0 and J_1 are parameters to be determined. These parameters remain constant with the concentration x, as can be see seen in Figs. 4 and 5 of Ref. 50.

Another expression for J used for the binary FeMn alloys $(q=0)$ in the fcc disordered phase is given by the dependence with Mn concentration x and discussed in,[12] namely,

$$J(x) = J_1 e^{xJ_0'}. \tag{30}$$

where J_0' is related with J_1 by the relation $J_0'=0.05J_1$.

Here, the order-parameter $m_1=m_2$, given in Appendix B, is related to the mean hyperfine field.[50] Figure 5 shows the experimental results of the reduced mean hyperfine field as a function of aluminum concentration q at room temperature for Fe concentration $p=0.50$ according to the data from Ref. 9. Note that the Mn concentration is given by $x=1-p-q$. In Fig. 5 it is also shown the previous theoretical fitting by using a simple Ising model from Ref. 12 (dashed line) together with a fitting by employing the present model (full line) with the following parameter values: Mn-Mn coupling $J_2 \equiv J_{\mathrm{MnMn}}=28.92\pm0.02$ meV; Fe-Mn coupling $J_4 \equiv J_{\mathrm{FeMn}}=14.54\pm0.02$ meV; Fe-Fe coupling $J \equiv J_{\mathrm{FeFe}}=-2.29\pm0.02$ meV; and $\Delta=2.5\pm0.1$ meV. The fittings have been obtained by numerically solving Eqs. (B7)–(B12) with $J_0=2.81J_1$ meV and $J_1=15.3$ meV in Eq. (29). In order to have as less theoretical parameter as possible, the values of J_0 and J_1 are the same as those used for the simple Ising

TABLE I. Values of the parameters J, J_2, J_4, and Δ according to the Blume-Capel (BC) model, Eq. (29), and also from the Ising (I) model of Ref. 12.

	J (meV)	J_2 (meV)	J_4 (meV)	Δ (meV)
I	0	15.3	9.6	
BC	-2.29 ± 0.02	28.92 ± 0.02	14.54 ± 0.02	2.5

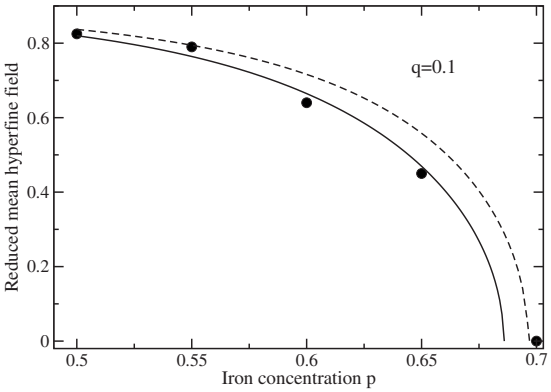

FIG. 6. Reduced mean hyperfine field as a function of Fe concentration p at room temperature for Al concentration $q=0.10$. Experimental data (full circles) are from Ref. 9 and the theoretical fitting from a simple Ising model (dashed line) are from Ref. 12. The solid line is obtained from the present Blume-Capel model with Eq. (29) and parameters given in the text.

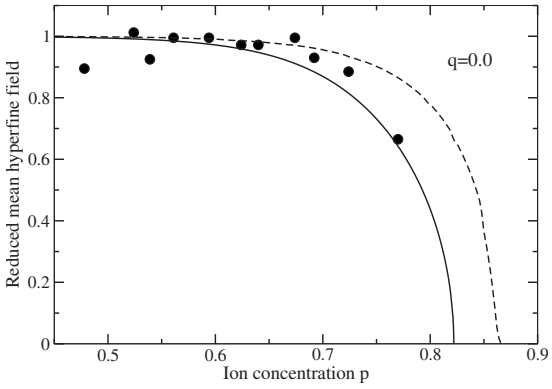

FIG. 8. Reduced mean hyperfine field as a function of Fe concentration p at room temperature for Al concentration $q=0$. Experimental data (full circles) are from Ref. 9 and the theoretical fitting from a simple Ising model (dashed line) are from Ref. 12. The solid line is obtained from the present Blume-Capel model with Eq. (30) and parameters given in the text.

system considered in Ref. 12. Differently from the previous fittings, where we have just used the theoretical parameters from Ref. 7 here we have tried some range of the parameters. So, the errors in the above parameters have been estimated in such a way that one does not have a significant visual difference of the corresponding theoretical curve. It can be noticed that both theoretical curves are almost equivalent when comparing to the experimental data. However, within the present approach, one gets a negative value for J, instead of zero interaction as in Ref. 12, which is certainly more plausible than no interaction at all between Fe atoms. Table I shows the present parameters in comparison to the previous ones.

Similarly, Figs. 6 and 7 show the reduced mean hyperfine field as a function of iron concentration p for two different Al concentrations, namely, $q=0.1$ and $q=0.05$, respectively. One can see that a rather better fitting is obtained for the Al concentration $q=0.1$ and that for $q=0.05$ both models give poor agreement with the experimental data. This is indeed a general trend with both models for small Al concentrations.

In order to get a further comparison for the FeMn binary system $(q=0)$ we have also considered the exchange behavior with Mn according to Eq. (30), where J_1 has the same value and J_0' has been changed. Figures 8 and 9 show the corresponding behavior of the exponential decay of the exchange coupling for $q=0.0$ by taking $J_0'=0$ and $J_0'=0.05J_1$, respectively (and the same value for J, J_2, and J_4). We can see that in both cases the fittings obtained by the present BC model are better than predicted by the simple Ising model.

VII. CONCLUDING REMARKS

The bond disordered Blume-Capel model has been used to describe the thermodynamic properties of FeNiMn and FeAlMn magnetic alloys through an approximate scheme based on a pair approximation. The agreement achieved from the present approach is far better than the previous one by taking a simple Ising model. Of course there is still the question regarding the applicability of such models since it has been known that they are suitable to describe the critical behavior of insulating anisotropic magnetic materials. However, as the situation for band magnets is still not so clear because of the lack of theoretical results on models that could be adequate to real experimental realizations, we believe that the BC, due to the present good fittings mainly for the spin-glass phase of FeNiMn alloys, will open a new venue for the application of such models to other magnetic systems.

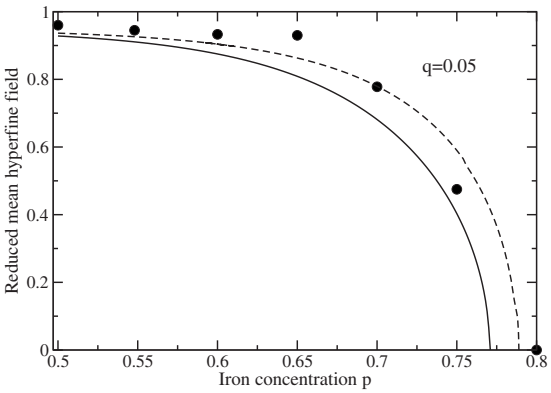

FIG. 7. The same as Fig. 6 for $q=0.05$.

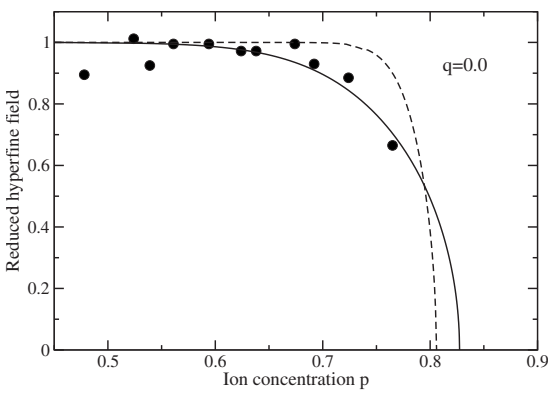

FIG. 9. The same as Fig. 8 for $J_0'=0.05J_1$.

APPENDIX A

In this Appendix we present the analytical results leading to the second-order ferromagnetic transition line as well as the Edwards-Anderson spin-glass transition line for the random-bond distribution (3).

In what follows we have:

$$\beta J_i = K_i, \quad d = \beta\Delta, \quad q_1 = z\beta\gamma, \quad q_2 = (z-1)\beta\gamma, \tag{A1}$$

$$I_0 = \sum_{i=1}^{z} K_i' b_i', \quad I_1 = \sum_{i=1}^{z-1} K_{1i} b_{1i}, \quad I_2 = \sum_{i=1}^{z-1} K_{2i} b_{2i},$$

$$Z_1 = 1 + 2\cosh(I_0), \quad Z_2 = 1 + 4e^{\delta_2} + 4e^{2\delta_2}\cosh(K_{12}). \tag{A2}$$

For the magnetizations and quadrupoles we obtain

$$m_1 = \frac{ze^{\delta_1}}{1+2e^{\delta_1}}, \tag{A3}$$

$$m_2 = (z-1)e^{\delta_2}\left(\frac{p^2 W_m(K)}{Z_2(K)} + \frac{q^2 W_m(K_1)}{Z_2(K_1)} + \frac{x^2 W_m(K_2)}{Z_2(K_2)} + \frac{2pqW_m(K_3)}{Z_2(K_3)} + \frac{2pxW_m(K_4)}{Z_2(K_4)} + \frac{2qxW_m(K_5)}{Z_2(K_5)}\right), \tag{A4}$$

$$Q_1 = \frac{e^{\delta_1}}{1+2e^{\delta_1}}, \tag{A5}$$

$$Q_2 = \frac{p^2 W_q(K)}{Z_2(K)} + \frac{q^2 W_q(K_1)}{Z_2(K_1)} + \frac{x^2 W_q(K_2)}{Z_2(K_2)} + \frac{2pqW_q(K_3)}{Z_2(K_3)} + \frac{2pxW_q(K_4)}{Z_2(K_4)} + \frac{2qxW_q(K_5)}{Z_2(K_5)}, \tag{A6}$$

where

$$W_m(K) = 1 + e^{\delta_2}\cosh(K) + 2e^{\delta_2}\sinh(K), \tag{A7}$$

$$Z_2(K) = 1 + 4e^{\delta_2} + 4e^{2\delta_2}\cosh(K), \tag{A8}$$

$$W_q(K) = 1 + 2e^{\delta_2}\cosh(K). \tag{A9}$$

For the Edwards-Anderson spin-glass parameter we get

$$h_1 = \frac{ze^{2\delta_1}}{(1+2e^{\delta_1})^2}, \tag{A10}$$

$$h_2 = (z-1)e^{2\delta_2}\left(p^2\frac{W_s(K)}{Z_2^2(K)} + q^2\frac{W_s(K_1)}{Z_2^2(K_1)} + x^2\frac{W_s(K_2)}{Z_2^2(K_2)} + 2pq\frac{W_s(K_3)}{Z_2^2(K_3)} + 2px\frac{W_s(K_4)}{Z_2^2(K_4)} + 2qx\frac{W_s(K_5)}{Z_2^2(K_5)}\right), \tag{A11}$$

$$R_1 = \frac{e^{2\delta_1}}{(1+2e^{\delta_1})]^2}, \tag{A12}$$

$$R_2 = e^{2\delta_2}\left(p^2\frac{W_q^2(K)}{Z_2^2(K)} + q^2\frac{W_q^2(K_1)}{Z_2^2(K_1)} + x^2\frac{W_q^2(K_2)}{Z_2^2(K_2)} + 2pq\frac{W_q^2(K_3)}{Z_2^2(K_3)} + 2px\frac{W_q^2(K_4)}{Z_2^2(K_4)} + 2qx\frac{W_q^2(K_5)}{Z_2^2(K_5)}\right), \tag{A13}$$

where

$$W_s(K) = 1 + 4e^{\delta_2}\cosh(K) + 8e^{2\delta_2}\cosh(2K). \tag{A14}$$

APPENDIX B

The pair approximation (PA) based on Bogoliubov inequality for the free energy[15] follows closely the procedure by Ref. 44. The single and pair of spins Hamiltonians are, respectively, given by

$$H_1 = -\gamma_s\sigma_1 - \delta_s\sigma_1^2 + \Delta\sigma_1^2, \tag{B1}$$

$$H_2 = -J_{ij}\sigma_1\sigma_2 - \gamma_p(\sigma_1+\sigma_2) - \delta_p(\sigma_1^2+\sigma_2^2) + \Delta(\sigma_1^2+\sigma_2^2), \tag{B2}$$

where γ_s, δ_s, γ_p, and δ_p are variational parameters to be determined from the condition of minimizing the free-energy

$$\mathcal{F} \equiv F/N = -\frac{z}{2}k_BT\ln(Z_2) - (1-z)k_BT\ln(Z_1) + (1-z)(\gamma_s m + \delta_1 Q) + z(\gamma_p m + \delta_2 Q), \tag{B3}$$

where $z=12$ for fcc and Z_1 and Z_2 are, respectively, the partition functions for single spins and pair of spins

$$Z_1 = \mathrm{Tr}[e^{-\beta H_1}], \quad Z_2 = \mathrm{Tr}[e^{-\beta H_2}]. \tag{B4}$$

The mean values $m=\overline{\langle\sigma\rangle}$ and $Q=\overline{\langle\sigma^2\rangle}$ are obtained from Hamiltonians H_1 and H_2, i.e.,

$$m(\gamma_s,\delta_s) \equiv \overline{Z_1^{-1}\,\mathrm{Tr}[\sigma_1\exp^{-\beta H_1}]} = \frac{1}{2}\overline{Z_2^{-1}\,\mathrm{Tr}[(\sigma_1+\sigma_2)e^{-\beta H_2}]}, \tag{B5}$$

$$Q(\gamma_p,\delta_p) \equiv \overline{Z_1^{-1}\,\mathrm{Tr}(\sigma_1^2 e^{-\beta H_1}]} = \frac{1}{2}\overline{Z_2^{-1}\,\mathrm{Tr}[(\sigma_1^2+\sigma_2^2)e^{\beta H_2}]}, \tag{B6}$$

where the configurational average is over the probability distribution given by Eq. (4). In this case, the minimization of the free energy with respect to the variational parameters leads to

$$(z-1)\gamma_1 = z\gamma_2, \quad (z-1)\delta_1 = z\delta_2. \tag{B7}$$

Equations (B4)–(B6) with the condition (B7) are equivalent to the Bethe approximation.[37] Below we have the expressions for the magnetizations. In what follows one has

$$r = \frac{z-1}{z}, \quad d = \beta\Delta, \quad K = \beta J,$$

$$a = \beta\gamma_1 \quad b = \beta\gamma_2. \tag{B8}$$

Magnetization

$$m_1 = \frac{e^{b-d}\sinh(a)}{1+2e^{b-d}\cosh(a)}, \tag{B9}$$

$$m_2 = \left\{ p^2 \frac{e^{rb+\lambda K}[e^d + 2e^{rb+\lambda K}\cosh(ra)]}{Z_{2p}} + x^2 \frac{e^{rb+\alpha K}[e^d + 2e^{rb+\alpha K}\cosh(ra)]}{Z_{2x}} + 2px \frac{e^{rb+\eta K}[e^d + 2e^{rb+\eta K}\cosh(ra)]}{Z_{2px}} q(2 - q)\frac{e^{rb}}{Z_{2q}} \right\} \sinh(ra). \tag{B10}$$

Quadrupole

$$Q_1 = \frac{e^{b-d}\cosh(a)}{1+2e^{b-d}\cosh(a)}, \tag{B11}$$

$$Q_2 = \frac{p^2}{2}\left\{1 - \frac{e^{d+\lambda K}[e^d + 2e^{rb}\cosh(ra)]}{Z_{2p}}\right\} + \frac{x^2}{2}\left\{1 - \frac{e^{d+\alpha K}[e^d + 2e^{rb}\cosh(ra)]}{Z_{2x}}\right\} + px\left\{1 - \frac{e^{d+\eta K}[e^d + 2e^{rb}\cosh(ra)]}{Z_{2px}}\right\} + q(2-q)\frac{e^{rb}\cosh(ra)}{Z_{2q}}, \tag{B12}$$

where

$$Z_{2p} = 2e^{2rb} + e^{d+\lambda K}[e^d + 4e^{rb}\cosh(ra)] + 2e^{2(rb+\lambda K)}\cosh(2ra), \tag{B13}$$

$$Z_{2x} = 2e^{2rb} + e^{d+\alpha K}[e^d + 4e^{rb}\cosh(ra)] + 2e^{2(rb+\alpha K)}\cosh(2ra), \tag{B14}$$

$$Z_{2px} = 2e^{2rb} + e^{d+\eta K}[e^d + 4e^{rb}\cosh(ra)] + e^{2(rb+\eta K)}\cosh(2ra), \tag{B15}$$

$$Z_{2q} = e^d + 2e^{rb}\cosh(ra). \tag{B16}$$

The above procedure has been done for the ferromagnetic model. Nevertheless, the same equations are obtained for the antiferromagnetic case where m_1 and m_2 are treated as sublattice magnetizations.

*Corresponding author. FAX: +57-2-339 3237; penalara@univalle.edu.co

[1] D. J. Chakrabarti, Metall. Trans. B **8**, 121 (1977).
[2] A. S. Hamada, L. P. Karjalainen, and M. C. Somani, Mat. Sci. Eng. A **431**, 211 (2006).
[3] A. S. Hamada, L. P. Karjalainen, and M. C. Somani, Mat. Sci. Eng. A **467**, 114 (2007).
[4] M. Shiga, T. Satake, Y. Wada, and Y. Nakamura, J. Magn. Magn. Mater. **51**, 123 (1985).
[5] B. Huck and J. Hesse, J. Magn. Magn. Mater. **78**, 247 (1989).
[6] J. Hesse, Hyperfine Interact. **47**, 357 (1989).
[7] A. Bohórquez, L. E. Zamora, and G. A. Pérez Alcazar, Phys. Rev. B **49**, 16035 (1994).
[8] G. A. Pérez Alcázar, J. A. Plascak, and E. Galvão da Silva, Phys. Rev. B **38**, 2816 (1988).
[9] G. A. Pérez Alcázar, E. Galvão da Silva, and C. Paduani, Hyperfine Interact. **66**, 221 (1991).
[10] L. E. Zamora, G. A. Pérez Alcázar, A. Bohórquez, and J. A. Tabares, J. Magn. Magn. Mater. **137**, 339 (1994).
[11] J. Restrepo, G. A. Pérez Alcázar, and J. M. Gónzalez, J. Appl. Phys. **87**, 7425 (2000).
[12] A. Osorio, E. Zamora Ligia, and G. A. Pérez Alcázar, Phys. Rev. B **53**, 8176 (1996).
[13] A. Osorio, W. R. Aguirre Contreras, L. E. Zamora, G. A. Pérez Alcázar, and J. A. Plascak, Phys. Rev. B **68**, 024420 (2003).
[14] J. A. Plascak, L. E. Zamora, and G. A. Pérez Alcázar, Phys. Rev. B **61**, 3188 (2000).
[15] H. Falk, Am. J. Phys. **38**, 858 (1970).
[16] A. R. Rivera, G. A. Pérez Alcázar, and J. A. Plascak, Phys. Rev. B **41**, 4774 (1990).
[17] J. A. Plascak, W. Figueiredo, and B. C. S. Grandi, Braz. J. Phys. **29**, 519 (1999).
[18] S. Kobe, Braz. J. Phys. **30**, 649 (2000).
[19] For additional applications of the Ising model to real materials see W. P. Wolf, Braz. J. Phys. **30**, 794 (2000).
[20] J. H. Van Vleck, Phys. Rev. **41**, 208 (1932).
[21] J. H. Van Vleck, *The Theory of Electric and Magnetic Susceptibilities* (Oxford University Press, New York, 1932).
[22] H. Bethe, Ann. Phys. **395**, 133 (1929).
[23] G. Christou, D. Gatteschi, D. N. Hendrickson, and R. Sessoli, MRS Bull. **25**, 66 (2000).
[24] R. M. Bozorth, *Ferromagnetism* (IEEE, Inc., New York, 1978), Chap. 12.
[25] R. C. O'handley, *Modern Magnetic Materials: Principles and Applications* (John Wiley & Sons, Inc., New York, 2000), Chap. 6.
[26] M. Blume, Phys. Rev. **141**, 517 (1966).
[27] H. W. Capel, Physica (Amsterdam) **32**, 966 (1966).
[28] H. B. Callen and J. Callen, J. Phys. Chem. Solids **27**, 1271 (1966).
[29] B. D. Cullity, *Introduction to Magnetic Materials* (Addison Wesley Pub. Co., Reading, MA, 1972), Chap. 7.
[30] V. A. Schmidt and S. A. Friedberg, Phys. Rev. B **1**, 2250 (1970).
[31] M. Blume, V. J. Emery, and R. B. Griffths, Phys. Rev. A **4**, 1071

(1971).
[32] A. M. Goldman, Phys. Rev. Lett. **30**, 1038 (1973).
[33] N. Giordano and W. P. Wolf, Phys. Rev. Lett. **35**, 799 (1975).
[34] A. K. Jain and D. P. Landau, Phys. Rev. B **22**, 445 (1980).
[35] O. F. de Alcántara Bonfim and C. H. Obcemea, Z. Phys. B **64**, 469 (1986).
[36] D. Peña Lara and J. A. Plascak, Mod. Phys. Lett. B **10**, 1067 (1996).
[37] D. Peña Lara and J. A. Plascak, Int. J. Mod. Phys. B **12**, 2045 (1998).
[38] F. C. Alcaraz, J. R. Drugowich de Felício, R. Köberle, and J. F. Stilck, Phys. Rev. B **32**, 7469 (1985).
[39] J. C. Xavier, F. C. Alcaraz, D. Peña Lara, and J. A. Plascak, Phys. Rev. B **57**, 11575 (1998).
[40] J. O. Indekeu, A. Maritan, and A. L. Stella, Phys. Rev. B **35**, 305 (1987).
[41] K. Croes and J. O. Indekeu, Mod. Phys. Lett. B **7**, 699 (1993).
[42] O. F. de Alcantara Bonfim, Physica A **130**, 367 (1985).
[43] W. Figueiredo and B. C. S. Grandi, Braz. J. Phys. **30**, 58 (2000).
[44] L. G. Ferreira, S. R. Salinas, and M. J. Oliveira, Phys. Status Solidi B **83**, 229 (1977).
[45] D. Peña Lara, J. A. Plascak, and J. Ricardo de Souza, Int. J. Mod. Phys. B **12**, 1813 (1998).
[46] M. L. Lyra and S. Coutinho Physica A **155**, 232 (1989).
[47] Ligia E. Zamora, G. A. Perez Alcazar, A. Bohorquez, A. Rosales Rivera, and J. A. Plascak, Phys. Rev. B **51**, 9329 (1995).
[48] V. O. Özçelik and A. Nihat Berker, Phys. Rev. E **78**, 031104 (2008).
[49] See *Fundamental Problems in Statistical Mechanics IV*, Proceedings of the International Summer School, Jadwisin, Poland, 1977, edited by E. G. D. Cohen and W. Fiszdon (1978), pp. 147–188.
[50] G. A. Pérez Alcázar, J. A. Plascak, and E. Galvão da Silva, Phys. Rev. B **34**, 1940 (1986).